J. Indian Inst. Sci., Nov.–Dec. 2001, **81**, 675–700

IISc THESES ABSTRACTS

Thesis Abstract M.Sc. (Engng)

Dynamic analysis and simulation of combdrive structures for MEMS by S. Pandari Nath
Research supervisor: Dr Rudra Pratap
Department: Mechanical Engineering

Elastic-electrostatic problem

Elastic-electrostatic problem arises in those systems where a mechanical structure is actuated through electrostatic forces. Electrostatic forces depend on displacement (geometry of charged bodies) and time. Basically, elastic-electrostatic problem combines general elastic problem with electrostatic field problem (Fig. 1).

Figure 1a describes the general elastic problem, where an elastic body is subjected to body forces, surface forces (T_1, T_2, T_S) and geometric constraints from boundary conditions. The goal is to find the stresses, strains and displacements of the elastic body.

Electrostatic problems deal with electrically conducting bodies. These problems often reduce to finding out potential field between two charged bodies. Once the potential field is found, it can be used to get any other information we desire about the electrostatic field at a point.

The elastic-electrostatic problem domain contains two charged bodies—one of them is a deformable elastic body with some geometric restraints, while the other is totally restrained and can be modeled as a rigid fixed body. Stresses, strains and deformations of the elastic body under electrostatic force are the quantities of interest. It is a two-way coupling problem, since the deformations is the elastic body and the electrostatic field depend on each other. A change in the electric field causes deformation of the elastic body and this deformation changes the electrostatic field between them. The final configuration achieved by the bodies should satisfy both the governing equations of mechanics as well as the electrostatic field equations.

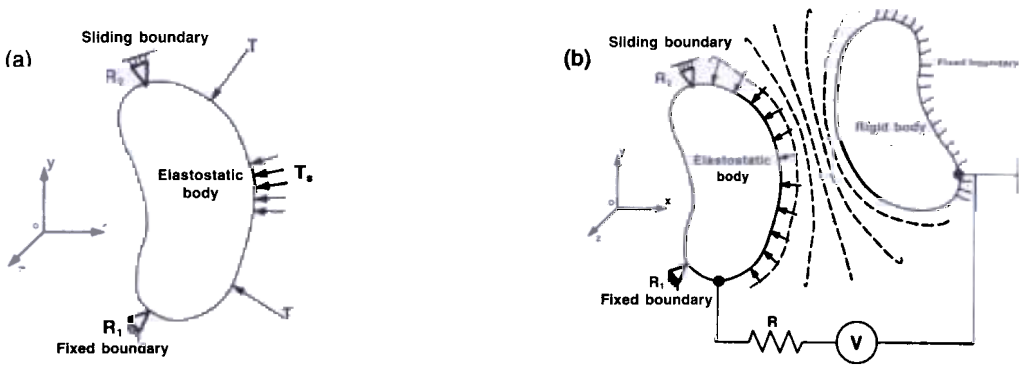

FIG. 1. (a) General elastic problem and (b) elastic-electrostatic problem.

2. A lumped parameter model for elastic-electrostatic problem

For elastic-electrostatic systems there are two governing equations, one for the mechanical structure in motion and the other for the resistor–capacitor circuit. MEMS devices are simple mechanical structures made up of an array of beams. Generally, the mechanical system is modeled as a spring–mass system. Diagrams of mechanical and electrical systems of interest are shown in Fig. 2. Figure 2a shows a spring-mass model of a MEMS structure under electrostatic actuation. M, K and $C(x)$ are system mass, effective stiffness of structure and capacitance between the two charged surfaces, respectively. The electrical circuit is shown in Fig. 2b, where R is the circuit resistance, $V(t)$, the applied voltage across the two bodies and $C(x)$, the displacement-dependent capacitance between the two charged bodies.

We use energy method described by Crandall *et al.*[1] to derive the governing equations. The method begins with an expression for the Lagrangian for the system

$$\mathcal{L}(x, \dot{x}, q, \dot{q}) = T^* - V \quad W_e \tag{1}$$

where T^*, V, and W_e are respectively the kinetic energy, the potential energy for the mechanical system and the potential energy for the electrical system. Expanding (1) and solving Lagrangian equation, we get

$$m\frac{d^2x}{dt^2} + b\frac{dx}{dt} + kx - \frac{1}{2}\frac{q^2}{C(x)^2}\frac{dC(x)}{dx} = 0 \tag{2}$$

$$R\frac{dq}{dt} + q\frac{1}{C(x)} = V(t) \tag{3}$$

Equations (2) and (3) model the mechanical and electrical subsystem of the system. The assumption typically employed in these coupled systems is that the time required for the capacitor to approximately change or discharge is an order of magnitude less than the period of oscillation of the mechanical system.

3. Numerical approach for coupled electromechanical systems

A combined finite-element/finite-difference (FE-FD) formulation for dynamic analysis of electrostatic comb sensor and actuator structures has been done with an iterative scheme. Figure 3

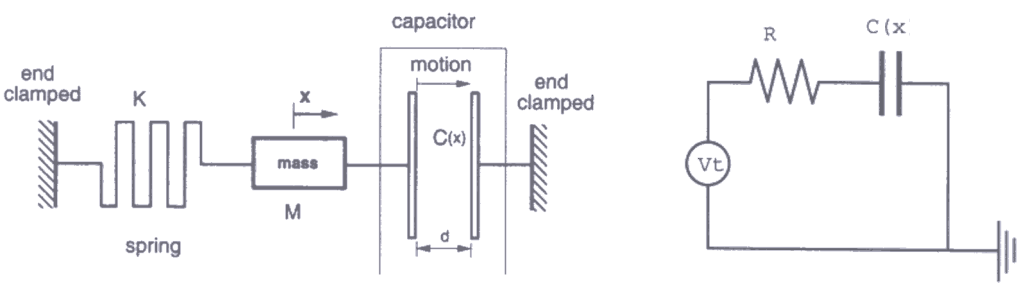

FIG. 2. A spring mass system actuated by a parallel plate capacitor (left). A voltage difference is applied between the two halves of the parallel plate. RC circuit for the electromechanical system is shown on the right.

shows the program structure. The dotted boundaries separate the two physical domains–electrical and mechanical.

In the absence of the electrical field, the dotted boundary on the right (mechanical) in Fig. 3 will be able to solve the governing differential equations of the structure with some force boundary conditions. Change in parameters of one domain causes change in parameters of the other domain. Hence the governing differential equations are solved by iterating between electrical and mechanical domains at each time step $(t+\delta t)$. The differential equations of motion are placed within the mechanical domain in the block diagram, as we neglect changing and discharging time of the capacitor.

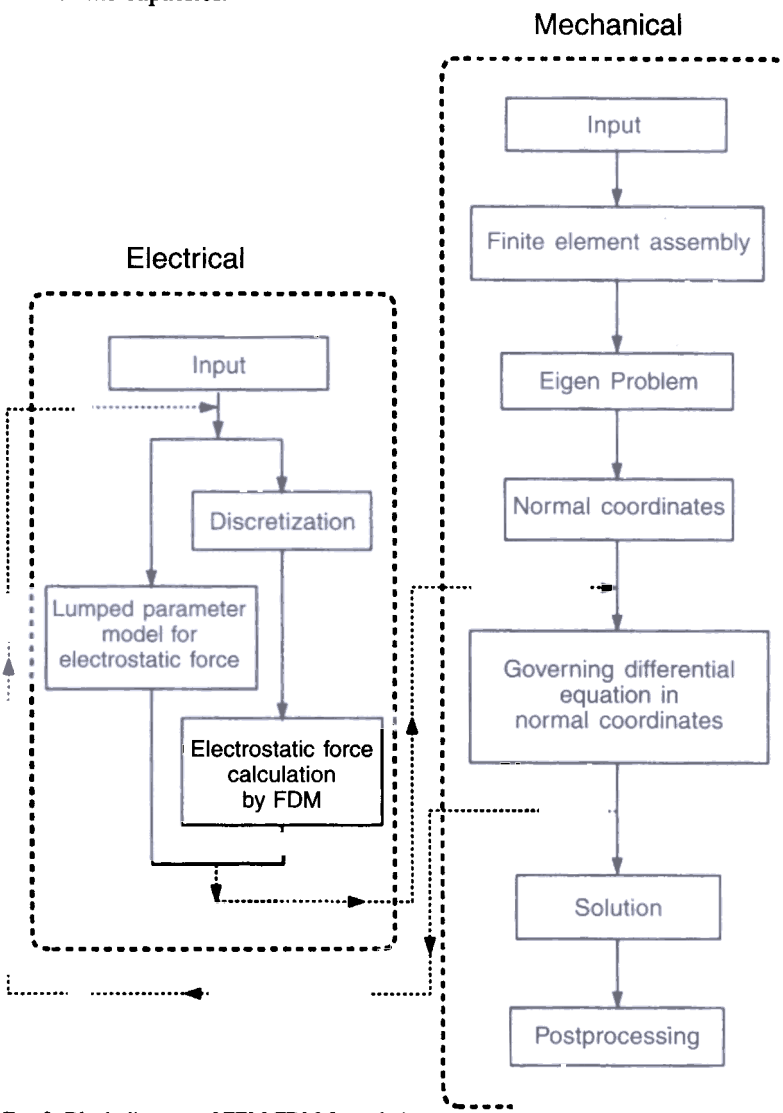

FIG. 3. Block diagram of FEM-FDM formulation.

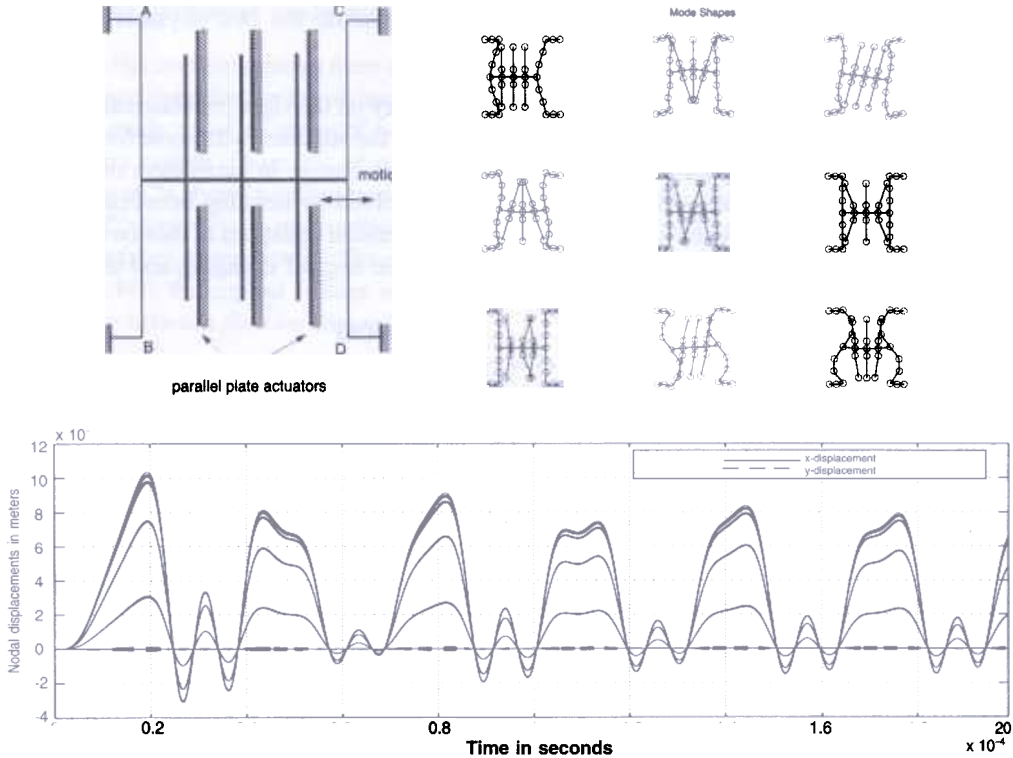

FIG. 4. Dynamic response of the microstructure due to the electrostatic parallel plate actuation.

4. Results

Figure 4 shows the results obtained for the structure shown in its top left corner. The structure consists of two fixed–fixed beams with end supports, attached through a relatively thicker beam. The parallel plate electrostatic actuation is used to excite the structure. Some of the lower mode shapes of the structure are also shown in the figure. The time history of nodal displacements of the discretized structure is obtained from normal-mode method of dynamic analysis. Modal truncation is used. In this case, first twenty mode-shapes are used for modal superposition. An AC voltage is applied between the two plates of the parallel plate actuators. The electrostatic force developed from the actuators depends on time as well the displacement of the structure.

References

CRANDALL, S. H., KARNOOP, D. C. KURTZ, E. F. JR AND PRIDMORE BROWN, D. C. — *Dynamics of mechanical and electromechanical systems,* McGraw-Hill, 1986.

NABORS, K. AND WHITE, J. — FastCap: A multipole accelerated 3-D capacitance extraction program, *IEEE Trans.,* 1991, **CAD-10**, 1447–1459.

3. SHI, F., RAMESH, P. AND MUKHERJEE, S. — Simulation methods for micro-electro-mechanical structures (MEMS) with application to a microtweezer, *Computers Struct.,* 1995, **56**, 769–783.

Thesis Abstract (Ph. D.)

Guanylyl cyclase C receptor: Regulation by protein kinase C by Nivedita Roy
Research supervisor: Prof. Sandhya S. Visweswariah
Department: Molecular Reproduction, Development and Genetics.

1. Introduction

Guanylyl cyclase C (GCC) is a membrane-bound guanylyl cyclase present predominantly on the apical surface of the intestinal villus cells. GCC binds ligands such as the heat-stable enterotoxin peptide (ST) and the endogenous ligands, guanylin, uroguanylin and lymphoguanylin. Ligand binding to the extracellular domain of the receptor activates its cytoplasmic catalytic domain to elevate intracellular cGMP leading to the activation of and subsequent opening of the chloride channel, cystic fibrosis transmembrane conductance regulator, CFTR. Opening of the CFTR is followed by secretion of chloride ion and water into the intestinal lumen and excessive chloride secretion results in water diarrhoea. The ST peptide mimics the signalling cascade triggered by guanylin/uroguanylin binding to GCC.[1,2]

2. Results and discussion

Guanylin, the first of the endogenous ligands discovered for GCC, is a 15-amino acid peptide isolated initially from the rat jejunum and identified as a ligand for GCC based on its ability to enhance cGMP levels in the T84 human colonic carcinoma cell line.[2] Studies were initiated to elucidate the mechanism and regulation of guanylin–GCC interaction and understand the physiological relevance of GCC-mediated signalling. Towards this end, a 15-amino acid sequence corresponding to the bioactive human guanylin was synthesized. Synthetic human guanylin was purified and air-oxidised to generate the bioactive peptide. Synthetic guanylin was able to bind and stimulate GCC in T84 cell in dose-dependent manner with an affinity of 50 nM, which was 100-fold lower than the affinity of GCC for STh.

Receptor activity is also regulated by the ability of the ligand to induce receptor desensitisation. *In vitro,* preincubation of GCC with STh, in the absence of the substrate Mg-GTP resulted in the inactivation of GCC. Synthetic human guanylin like STh was able to induce inactivation of GCC in T84 membranes. However, at equimolar concentrations, guanylin induced a lower extent of inactivation of GCC when compared to STh-induced inactivation. This could be explained on the basis of receptor occupancy and the affinities of the ligands for GCC, since receptor activation and its inactivation both require ligand binding. Therefore, guanylin induced changes in receptor conformation resulting in both activation and inactivation in a manner similar to ST, suggesting that guanylin is a full agonist for GCC.[3]

It was clear that guanylin because of its 100-fold lower affinity for GCC, at a physiological concentration, would not cause a significant increase in intracellular cGMP in the intestinal cells. It was therefore envisaged that guanylin bioactivity could be potentiated by cross-talk with other signalling pathways. Regulation of STh-stimulatable activity by PKC-mediated phosphorylation of GCC at a critical ser-1029 has been reported. Therefore, the potentiation of PKC activation as a possible mechanism for enhanced guanylin-mediated GCC activity was investigated.[3]

T84 cells were treated with the potent PKC activator, phorbol myristate acetate (PMA), prior to the addition of guanylin. There was a 2.6-fold enhancement in guanylin-induced cGMP levels upon PMA treatment of T84 cells. An important observation was that basal cGMP levels remained unchanged. PMA-mediated potentiation of guanylin-induced GCC activity was significantly inhibited by preincubation of T84 monolayers with staurosporine, a potent inhibitor of PKC, indicating that a phosphorylation-mediated mechanism was operative.[3]

Interestingly, PMA-mediated potentiation of guanylin bioactivity was mimicked by carbachol, a cholinergic agonist that activated PKC via activation of PLCβ and release of diacylglycerol. This was important as it suggested the possibility that cross-talk with signalling pathways that activated PKC could indeed potentiate guanylin-induced GCC activity *in vivo*.

The enhancement of ligand-induced GCC activation was not due to increased ligand binding to the receptor, as no significant increase was observed in either the affinity or the binding sites of GCC for guanylin on PMA treatment. This indicated that the modulation of the catalytic domain of GCC was responsible for increase in cGMP levels subsequent to ligand binding. Moreover, ligand-induced inactivation was not alleviated in PMA-treated cells, suggesting distinct mechanisms for ligand-induced activation and inactivation.[3]

One of the characteristic features of PMA-mediated regulation of PKC is the downregulation of PKC activity upon prolonged exposure to PMA. However, in contrast with the potentiation observed in ligand-stimulated GCC activity on exposure of T84 cells to PMA, both the basal- and the ligand-induced GCC activity was inhibited by 50% upon prolonged exposure to PMA. Additionally, equilibrium-binding data and Western Blot analysis using GCC-Specific monoclonal antibody revealed a reduction in total receptor content upon prolonged PMA treatment. It was possible therefore that the decrease in GCC content observed on prolonged PMA treatment was a reflection of reduced levels of GCC mRNA.

Northern analysis of GCC mRNA from T84 cells treated with PMA for various time periods showed a decline in the steady-state levels of GCC mRNA. The GCC mRNA levels were compared with the GCC protein content in T84 cells treated with PMA. There were several interesting inferences from this analysis. At the end of 1 h of PMA treatment, though the ligand-induced GCC activity was potentiated with no change in the receptor content, GCC mRNA levels reduced by 35%. Therefore, there was a dual and contrasting regulation of GCC by PKC on short-term PMA treatment. Staurosporine could completely reverse the PMA-mediated downregulation of GCC, proving conclusively that the reduction in GCC mRNA was due to a PKC-mediated phosphorylation event. Carbachol also mimicked the phorbol ester-mediated downregulation of GCC mRNA. The carbachol-mediated downregulation was reversed by staurosporine suggesting that PKC-mediated downregulation of GCC mRNA could be initiated via signalling mechanism that activates PKC under physiological conditions.

Reduction in steady-state levels of mRNA could be either due to increases in the rate of mRNA degradation and/or because of decreases in the rate of transcription of GCC gene. To exclusively monitor the rate of degradation of GCC mRNA, control and PMA-treated T84 monolayers were incubated with actinomycin D for various times. No change in the rate of degradation of GCC mRNA was observed but run-on analysis performed on nuclei prepared from control and PMA-treated T84 cells showed a 70% decrease in GCC transcription.

One of the mechanisms of transcriptional downregulation of GCC could be through differential binding of transcription factors to their target sites in the GCC promoter in control and PMA-treated cells. In the 1.8 kb known promoter of the GCC gene, there are binding sites present for several transcription factors including Cdx2, hepatic nuclear factor (HNF4) and GATA-4.[4] However, known phorbol ester-responsive was missing in the GCC promoter. It was conceivable that PKC could mediate changes in the phosphorylation status of Cdx2, HNF4 or GATA and thereby regulate their DNA binding activity. The multiple Cdx2 and GATA binding and one of the four HNF4 binding sites present in the GCC promoter are identical with known consensus, binding sites for these factors. Modulation of activity of the transcription factors on PMA treatment of T84 cells was investigated by monitoring the binding of these transcription factors to their cognate sites in electrophoretic mobility shift assays (EMSA).

Oligonucleotides corresponding to consensus target sites for Cdx2, HNF4 and GATA were synthesized. Results of the EMSA using the consensus binding sites for Cdx2, GATA and HNF4 demonstrated the presence of these transcription factors in T84 cells. Upon PMA treatment and activation of PKC, there was a dramatic decrease in DNA binding in all the three transcription factors to their cognate sequence. Interestingly, there was a varying extent of recovery in DNA binding of these transcription factors upon inhibition of PKC activity. Staurosporine significantly reversed the reduction in DNA binding ability of Cdx2 and GATA by 60% and 75%, respectively, but recovery was only to 30% of control in the case of HNF4 binding to its cognate site. Therefore, it was possible that PMA not only triggered the activation of PKC but perhaps also other kinases such as PKA, which could in turn modulate HNF4 binding. Moreover, PMA addition appears to negatively modulate the activity of Cdx2, HNF4 and GATA at the same time, which emphasizes the hypothesis that perhaps GCC gene regulation is mediated by multiple factors binding to its upstream promoter sequence.

In view of the already established role of HNF4 in regulation of GCC transcription[5] it was important to investigate the mechanisms of PMA-mediated modulation of DNA binding activity of HNF4. It is possible that the observed reduction in DNA binding activity of HNF4 is either due to a reduction in total HNF4 protein content or a functional modulation of HNF4 activity. Western blot analysis of control and PMA-treated nuclear extract with HNF4-specific antibody showed no reduction in HNF4 content. No difference in phosphorylation was observed upon ^{32}P labelling of control and PMA-treated T84 cells and subsequent immunopecipitation of HNF4 protein from the nuclear extracts. Therefore, it was not a direct regulation of HNF4 on PMA treatment that modulated its DNA binding activity. However, the possibility that the PMA-mediated regulation of DNA binding activity of HNF4 could occur through phosphorylation of an HNF4-associating factor could not be entirely ruled out.

3. Conclusion

The studies in this work attempt to delineate the mechanisms of transcriptional and posttranscriptional regulation of GCC by PKC. PKC-potentiated ligand induced GCC activity but downregulated GCC transcription allowing finetuning of the regulation of GCC-mediated signalling. The results reported suggest the possibility of *in vivo* regulation of GCC by cross-talk with numerous pathways that are reported to activate PKC. Studies on regulation of GCC transcription could provide an insight into the variety of mechanisms employed by organisms to maintain tissue-specific gene expression.

legume lectins, known so far, possess a similar tertiary fold, described as 'Jelly roll'. But they differ considerably in the modes of subunit association in thier quaternary structure. In concanavalin A (con A), pea and lentil lectin the subunits interact more extensively to form the 'canonical structure'. A relatively large surface area, 1000 Å, is buried at the intersubunit interface. On the other hand, in *Erytherina corralodendron* lectin (*Ecor*L) and WBA I, the subunits interact less extensively, with just 700 Å buried at the subunit interface. A consequence of these differences is observed when one compares the $\Delta H_J/\Delta H_v$ values of their thermal denaturation transitions. The canonically associated lectins possess a cooperativity ratio of one. When one considers that these are oligomeric proteins, this value suggests that the entire oligomeric structure of these lectins unfolds as a single entity and that their unfolding is indistinguishable from their subunit dissociation. On the other hand, both *Ecor*L and WBA I possess a cooperativity ratio of two. This immediately suggests that they possess two independently unfolding domains, which may be identified as their respective monomers. Differential scanning calorimetric studies on WBA II have shown that this protein possesses an unfolding cooperativity of two. One is thus tempted to suggest that WBA II may possess a similar subunit organisation as that of WBA I and *Ecor*L. Solution denaturation studies carried out in WBA II, as well as in con A and pea lectin, support this conclusion. Both stability and change in heat capacity upon unfolding is lower in WBA II than in con A and pea lectin. Since change in heat capacity is a measure of the extent of the buried hydrophobic core of a protein and since legume lectins possess a similar subunit structural fold, these differences perhaps reflect different modes of subunit association. WBA II may take on a quaternary association in which there is significantly less sequestration of the surfaces.

3d. Very interesting observations were made from solution denaturation studies on peanut agglutinin (PNA) that may have implications in protein folding as such, and more particularly, in the importance of the oligomeric assemblage in legume lectins. During the unfolding of PNA a molten globule like intermediate is formed. This intermediate is monomeric and binds analinonaphthelene sulfonate. Also, though nearly 80% of the secondary structural elements in the intermediate is in tact, it has lost nearly 70% of its tertiary structure. Yet, quite remarkably, despite this considerable loss in tertiary structure, this intermediate retains most of its ligand-binding capability. This immediately suggests that the monomers of legume lectins possess all the elements necessary for sugar recognition and that oligomerization imparts them overall stability and spatial disposition necessary for the manifestation of its biologic activity.

3e. WBA II was cloned by PCR of the genomic DNA and sequenced. Comparison of its amino acid sequence with those of other legume lectins has provided some insights into its structure and mechanism of ligand recognition. Many of the residues that are part of the β-sheet regions in legume lectins are conserved in WBA II. Also, all the residues required for metal ion binding appear to be conserved in WBA II as well. In addition, there is very good sequence conservation of the four loops that form the ligand-binding site in legume lectins. Yet, subtle differences have been noted which, perhaps, reflect the fine differences in ligand specificity of this lectin. WBA II exhibits greater anomeric discrimination than either peanut agglutinin and *Ecor*L, but lesser than that of WBA I. Whereas WBA I binds methyl-α-galactose 6–8 times as strongly as it does the β-anomer, PNA and *Ecor*L bind both, to almost the same extent. WBA II, on the other hand, binds methyl-α-galactose only about three times as strongly as it does the β counterpart. The large size

of the D-loop in WBA I appears to substantially hinder the binding of the β-anomer of methylgalactose. On the other hand, because of a smaller D-loop, the peanut agglutinin and *Ecor*L binding site is able to accommodate both the anomeric configurations. In WBA II, the size of the D-loop appears to be smaller than that of WBA I, and hence is less anomer specific than the latter. But the presence of the bulky tyrosine, at position 216, may provide some hindrance to the binding of β-anomer and consequently WBA II possesses greater anomeric specificity than *Ecor*L and peanut lectin.

References

SUROLIA, A., SHARON, N AND SCHWARZ, F. P. — *J. Biol. Chem.*, 1996, **271**, 17697–17703.

2. ACHRAYA, S. — *Characterisation of DNA ligase and pairing activities from a partially purified fraction from rat testis*, Ph. D. Thesis, Indian Institute of Science, Bangalore, India, 1992.

Thesis Abstract (Ph. D.)

Structural studies on peanut lectin–carbohydrate complexes by R. Ravishankar
Research supervisor: Prof. M. Vijayan
Department: Molecular Biophysics Unit

1. Introduction

Lectins are carbohydrate-binding proteins that specifically recognise diverse sugar structures and mediate a variety of biological processes such as cell–cell and host–pathogen interactions, serum glycoprotein turnover and innate immune responses.[1] There has been a spurt in lectin research in recent years on account of their ability to specifically bind to cell surface carbohydrates and in view of their diverse applications.[2] A rich source of lectins are the seeds of leguminous plants, but they are also found in all classes and families of organisms. Legume lectins have similar tertiary structures, but exhibit a large variation in their quaternary structures. The carbohydrate-binding site in all of them is made up of four loops. Three of the loops are substantially conserved in all legume lectins of known structure while the fourth loop, which is variable, is thought to confer specificity. Legume lectins which share the same monosaccharide specificity often exhibit markedly different oligosaccharide specificities.

The work is concerned with structural studies on the carbohydrate complexes of peanut (*Arachis hypogaea*) agglutinin (PNA), a nonglycosylated tetrameric lectin of M_r 110,000 Da with 236 amino-acid residues in each subunit. PNA specifically recognises the tumor-associated Thomsen–Friedenreich antigen (T-antigen; Galβ1-3GalNAc), at the disaccharide level.

2. Methods

Diffraction data from the complexes were collected on a Siemens–Nicolet area detector system mounted on a GX-20 Marconi avionics rotating anode X-ray generator and an MAR imaging plate system mounted on a Rigaku RU200 rotating anode generator. The data were processed using XENGEN, MAR-XDS and DENZO/SCALEPACK suites of programs. Molecular replace-

ment calculations were carried out using AMoRe. The refinements were performed using PROLSQ and X-PLOR.

3. Results and discussion

The observed variability in quaternary association in legume lectins was earlier thought to arise mainly due to the presence of covalently bound sugar at the intersubunit interface. The structure of PNA (a nonglycosylated protein) indicates that the observed variability in the quaternary association of legume lectins is caused by factors intrinsic to the protein itself.[3] At neutral pH, PNA exists as an 'open' tetramer with four identical polypeptide chains which does not exhibit the 222 (D_2) or the 4-fold (C_4) point group symmetry expected in a tetramer. The structure of its complex with lactose (Galβ1-4Glc) at 2.25 Å highlights the differences in carbohydrate binding between galactose/N-acetylgalactosamine-specific legume lectins as opposed to glucose/mannose-specific legume lectins.[4] The detailed analysis of the tertiary structure brings to focus the features of the legume lectin fold not appreciated sufficiently in earlier work. Furthermore, in legume lectins, more than 50% of the tertiary structure exists in loops. An analysis of protein hydration demonstrates, among other things, the role of water molecules in stabilising the structure of these loops.

The X-ray analysis of the complex with T-antigen shows that the 20 times higher affinity of the protein for T-antigen compared to that for lactose arises primarily on account of two additional water bridges.[5,6] The structures of N-acetyllactosamine (Galβ1-4GlcNAc) and methyl-β-glactose complexes and a comparative study involving these and the other complexes of the lectin indicate that the role of interacting sugar hydroxyls, when absent, is often mimicked by ordered water molecules not only at the primary combining site but also at the site of the second sugar ring in the lectin.[7] The similarity of peanut lectin–sugar interactions with those in other Gal/GalNAc-specific lectins extends to a substantial degree to water bridges as well. The study provides a structural explanation for the exclusive specificity of peanut lectin for galactose at the monosaccharide level as against that of the other lectins for galactose as well as N-acetylgalactosamine. The complexes also provide a qualitative structural rationale for differences in the strengths of the binding of peanut lectin to different sugars. The complex with C-lactose demonstrates unambiguously that the synthetic sugar mimics its natural counterpart in its interaction with PNA.[8]

The structures of the complexes of PNA with lactose at acidic pH were solved in a mono- and a triclinic form at resolutions of 2.6 and 3.5 Å, respectively (unpublished results). The tertiary and the quaternary structure of the lectin at this pH remains the same as that at physiological pH. The former contains two tetramers in the asymmetric unit. Sugar binding is observed in three subunits in this form. It is prevented in two subunits by interactions with neighboring molecules. Two other subunits have no sugar bound to them although the combining sites are accessible. Some water molecules at these sites occur close to the positions of carbohydrate hydroxyl groups in sugar-bound subunits. A loop in a neighbouring molecule binds to the carbohydrate-binding site in one subunit by partly mimicking the interactions of the glucose moiety in lactose. Furthermore, some of the oxygen atoms of this peptide stretch are topologically equivalent to some of the sugar hydroxyls. This same loop interacts in an analogous manner with the carbohydrate-binding site in two subunits in the triclinic form which contains a tetramer in the unit cell. It was

not possible to interpret the density (possibly for lactose) at the binding site of the other two subunits in this form on account of inferior resolution. The differences in the crystal packing between the orthorhombic, mono- and triclinic forms have been attempted to be rationalised based on the high affinity of the protein for the peptide loop at acidic pH.

4. Appendices

An Appendix reports the crystal structure determination of the key DNA repair enzyme from *E.coli* Uracil DNA glycosylase (UDGase) in its complex with a proteinaceous inhibitor.[9] Another is concerned with the X-ray structure determination of the complexes of DL- and L-arginine with maleic acid.[10]

References

	Lis, H. and Sharon, N.	*Chem. Rev.*, 1998, **98**, 637–674.
2.	Vijayan, M. and Nagasuma Chandra, R.	*Curr. Opin. Struct. Biol.*, 1999, **9**, 707–714.
3.	Banerjee, R. *et al.*	*Proc. Natn. Acad. Sci. USA*, 1994, **91**, 227–231
4.	Banerjee, R. *et al.*	*J. Mol. Biol.*, 1996, **259**, 281–269.
5.	Ravishankar, R., Ravindran, M. Suguna, K., Surolia, A. and Vijayan, M.	*Curr. Sci.*, 1997, **72**, 855–861
6.	Ravishankar, R., Ravindran, M. Suguna, K., Surolia, A. and Vijayan, M.	*Curr. Sci.*, 1999, **76**, 1393.
	Ravishankar, R., Suguna, K. Surolia, A. and Vijayan, M.	*Acta Cryst. D*, 1999, **55**, 1375–1382.
8.	Ravishankar, R., Surolia, A., Vijayan, M., Lim, S. and Kishi, Y.	*J. Am. Chem. Soc.*, 1998, **120**, 11297–11303.
9.	Ravishankar, R. *et al.*	*Nucl. Acids Res.*, 1998, **26**, 4880–4887.
10.	Ravishankar, R., Nagasuma Chandra, R. and Vijayan, M.	*J. Biomol. Struct. Dyn.*, 1998, **15**, 1093–1100.

Thesis Abstract (Ph. D.)

Analytical and neural network studies on higher harmonic control of helicopter by S. N. Omkar

Research supervisor: Prof. J. Nagabhushanam

Department: Aerospace Engineering

1. Introduction

The investigations on the determination and control of vibration involve solving the helicopter rotor-body equations of motion with constraints of specified flight conditions (trim). Though several schemes are available to computer trim, an effective method is yet to emerge. Higher

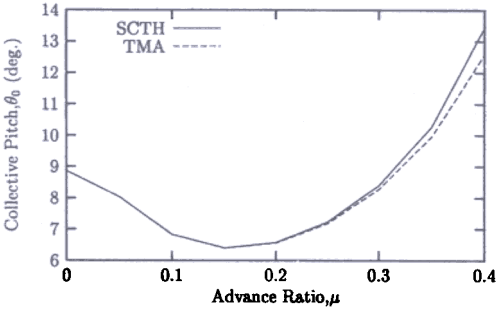

FIG. 1. Collective pitch with advance ratio (SCTH and TMA).

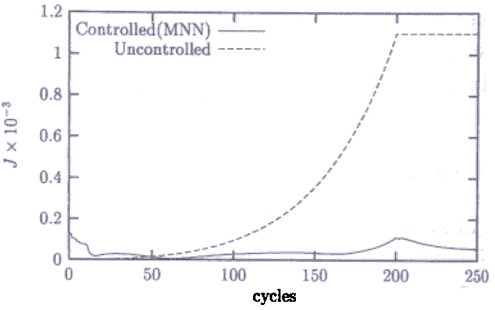

FIG. 2. Controlled J for varying forward speed.

harmonic control (HHC) is one of the active control methods available for minimization of vibration. Several analytical and experimental investigations have been made on HHC using the classical adaptive control techniques. With the development of neural network controllers, there seems to be a great potential in applying them for HHC of helicopter as well.

2. Trim and HHC

Studies on trim and HHC for minimization of helicopter vibration are carried out using Incremental Harmonic Balance Method (IHBM). This method has not yet been utilized for analytical investigations related to helicopter. A variation of this method, called Harmonic Correction Method (HCM), which reduces the computational time taken by the IHBM, is proposed. The use of IHBM/HCM, for computing trim and response, is demonstrated on three graded analytical models of rotor/rotor-body system. A comparison of the performance of IHBM/HCM is made with existing methods, namely, Periodic Shooting Method and Auto-Pilot Scheme, in terms of solution accuracy and computer time requirements.

The IHBM/HCM are extended for simultaneous computation of trim, response and HHC (SCTH) for hub shear minimization. The results of this are compared with the conventional T-matrix approach (TMA) in which the HHC are computed keeping a constant trim. The differences in results by adapting these two approaches are brought out. These studies indicate that IHBM/HCM are computationally efficient and are viable methods to compute trim, response and HHC for hub shear minimization. Further, the study brings out the necessity for considering simultaneous computation of the trim and HHC for high forward speeds. Figure 1 shows the collective pitch as computed by SCTH and TMA.

3. NN controller

A Neural Network (NN) architecture is used for the minimization of rotor hub shear forces through HHC. For this, a coupled rotor-body analytical model is considered as Multi-Input-Multi-Output (MIMO) system. First, the dynamics of this system, with HHC as inputs and hub shear forces as outputs, is identified using a series-parallel NN architecture. Later, Model Reference Adaptive Control (MRAC) architecture is employed to provide HHC inputs to the MIMO system for hub shear minimization. The identifier and controller architectures are based on Memory Neuron Network (MNN),[1] which is a type of recurrent neural network with built-in memory.

Extensive simulations are carried out on the NN identifier and controller and their performance is validated using the results obtained through analytical methods. These simulations indicate that the NN-based architectures are effective in minimizing hub shear forces through HHC. The fact that they can learn and adapt efficiently is also brought out. Figure 2 shows the controlled and uncontrolled force levels.

4. Fault tolerance

A new NN architecture is also proposed for sensor fault tolerance. This model, called Memory Auto-Associative Network (MAAN), is a hybrid of conventional Auto-Associative Network $(AAN)^2$ and MNN. Initially, two simple analytical models are considered to assess the relative performances of MAAN and AAN. The simulations prove the superiority of MAAN over AAN, as supported by theoretical analysis. MAAN can perform well even when measurements through redundant sensors are not available. Further, it can do better feature extraction while removing sensor bias and compensating for failed sensors. Later, the simulation studies for fault tolerance are extended to a typical rotor-body model. It is observed that MAAN can effectively filter noise, remove sensor bias and adequately compensate for the values of missing sensors.

5. Conclusions

The IHBM and HCM are viable methods for computing trim and HHC simultaneously. Further, they are computationally efficient and less expensive when compared to prevailing methods. Neural network-based architectures can be successfully employed for minimising hub shear forces. MAAN can considerably reduce the ill-effects of noise and bias while providing adequate compensation for failed sensor values.

References

SASTRY, P. S., SANTHARAM, G. AND UNNIKRISHNAN, K. P. — Memory neuron networks for identification and control of dynamical systems, *IEEE Trans.*, 1994, **NN-5**, 1–3.

KRAMER, M. A. — Autoassociative neural networks, *Computers Chem. Engng*, 1992, **16**, 313–328.

Thesis Abstract (Ph. D.

Computational analysis of ground effect on single and multi-element airfoils by J. Uma Maheswari

Research supervisors: Profs A. Prabhu and V. S. Holla, and Dr H. Kamath

Department: Aerospace Engineering

1. Introduction

The aim of the present study is to analyse the ground effect characteristics of single and multi-element airfoils. On examining the results of the previous investigators, it is seen that a detailed computational analysis of airfoils in ground effect, especially high-lift airfoils in ground effect, is lacking. Even though efforts have been made to explore the parameters which have direct influence on the aerodynamic characteristics of several configurations in close proximity to the

ground, the available information on the behavior of airfoils near ground is meagre. Furthermore, the few studies which have been reported on the computational analysis of viscous flows past airfoils near ground seem to have simulated the ground as a fixed plate. Consequently, these results correspond to merely a wall-interference study. The aims of the present work are:

1. Development of an efficient code for the study of inviscid and viscous flows past single and multielement airfoils.
2. Use of a proper surface boundary condition in order to correctly simulate the ground effect.
3. A systematic study of the several parameters influencing the ground effect.
4. A detailed analysis of viscous flow characteristics.
5. Effect of ground on the aerodynamics characteristics of a multielement airfoil.

For this purpose, a structured, patched, multiblock grid is generated around configurations of interest. The generation of multiblock grids is based on the elliptic grid generation technique. The governing equations are the steady compressible Navier–Stokes equations. In the present study, the inviscid fluxes are computed using a third-order accurate flux difference splitting scheme given by Roe and the viscous fluxes are computed using a central difference approach given by Peyret and Taylor. To obtain a steady-state solution, a pseudo time-step method based on six-stage Runge–Kutta method is applied.

2. Potential flow analysis

A potential flow analysis is carried out using surface singularity method for several symmetric and cambered airfoils. The ground is simulated by reflecting the airfoil using the method of images. For this analysis, a linearly varying vortex singularity has been used and extensive studies are made on the effect of ground on the lift coefficient of a variety of airfoils with a wide variation of geometric parameters, namely, thickness and camber. The results are shown in Fig. 1. From this study it has been observed that,

Increase in thickness increases the negative effect of ground.

Increase in camber results in positive ground effect.

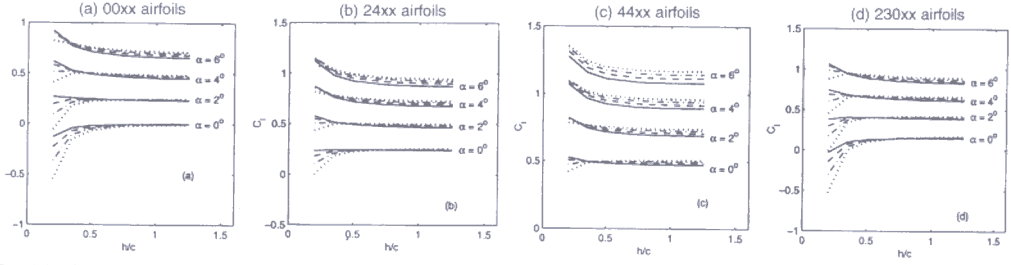

For (a), (b) and (c): – $t/c = 0.06$; –– $t/c = 0.09$; -.- $t/c = 0.12$; .... $t/c = 0.15$; For (d) : – $t/c = 0.12$; –– $t/c = 0.15$; -.- $t/c = 0.18$; .... $t/c = 0.21$.

FIG. 1. Potential flow analysis of ground effect on single airfoil

3. At higher angles of attack, pronounced ground effect is felt up to large ground heights.
4. Symmetric airfoil with a thickness $t/c > 9\%$ would experience a negative ground effect when $h/c \leq 0.4$ and $\alpha \leq 4$.
5. Cambered airfoils with a minimum of 4% camber will have a positive effect up to about 12% thickness.

3. Euler solutions

Next, Euler solutions are presented for NACA 0012 and NACA 4412 airfoils for different ground heights and angles of attack to analyse the effect of ground on the lift coefficient. The change in the surface pressure distribution is also discussed. Even though the configuration is a single airfoil, a multiblock grid is used since the ground has to be included. In general, the solutions of the Euler equations show similar trends as that of potential flow solutions. The Euler solutions also demonstrate that pronounced ground effect is felt even at large ground clearances when the angle of attack is higher and also that, on the ground, pressure/suction peaks occur at smaller angles of attack. Compared to potential flow solutions, the Euler solutions have the advantage of being used at subsonic compressible Mach numbers also.

4. Viscous flow analysis

The viscous flow past single airfoils in close proximity to the ground has been investigated using a multiblock grid and a finite-volume technique. A symmetric and a cambered configuration are considered at different ground heights and angles of attack for three different Reynolds numbers. A detailed study has been made to analyse the effect of ground on the various aerodynamic coefficients like pressure, skin friction, lift and drag. Figure 2 shows some typical variations of lift and drag coefficients for the viscous case.

One of the main aims is to emphasise the usage of an appropriate boundary condition for the ground effect studies. A thorough analysis shows that the boundary condition plays a significant role in the prediction of flow characteristics. It is shown that the no-slip condition results in very early separation and predicts higher drag coefficients than the slip condition. It is shown clearly that the two boundary conditions give substantial differences in the pressure distribution, lift and drag. Therefore, it is concluded that it is necessary to use the right boundary condition to get the correct results.

From the thorough studies made using the slip boundary condition on the ground, it can be concluded that, in the range of the parameters considered,

1. Separation is hastened by the proximity of ground.
2. The variation of lift and drag coefficients with respect to Reynolds number is nonlinear at all ground heights.
3. At a low ground height of $h/c = 0.2$, the effect of the ground is more positive at the low Reynolds number.
4. There is a lift loss near the ground with increase in Reynolds number.

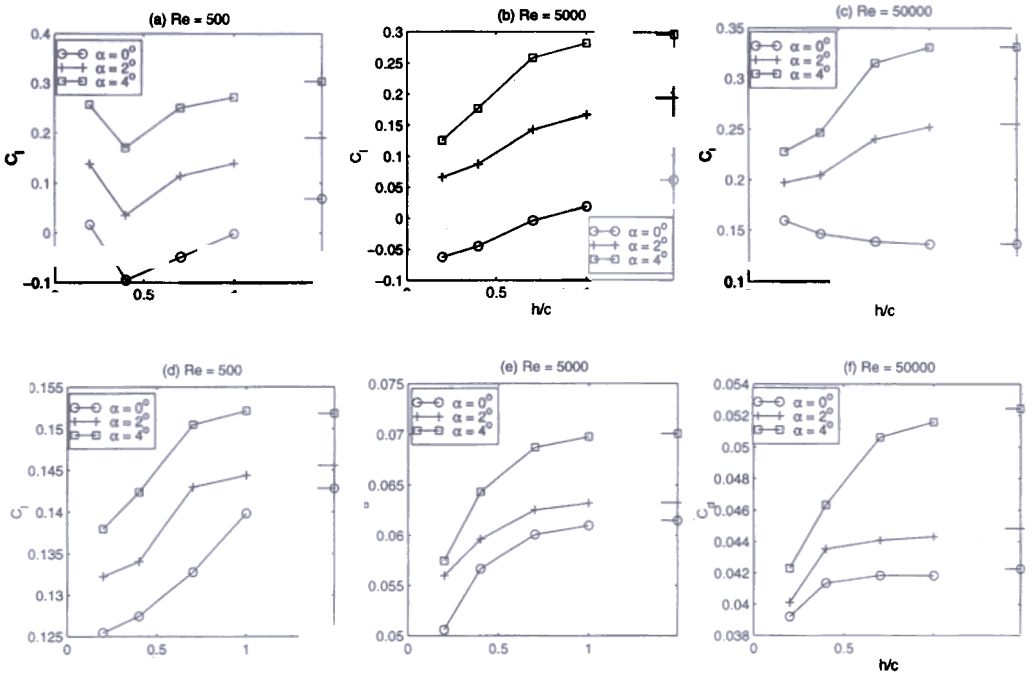

FIG. 2. Viscous flow analysis of ground effect on single airfoils.

5 The drag decreases as the ground height decreases

In the computational studies on ground effect by Hsuin *et al.*[1] it was shown that there is an increase in drag coefficient when the ground height decreases. In their study, the ground has been simulated as a fixed plate (by imposing the no-slip condition on the ground) which is rather a wall interference effect. Further, it was observed from the present study that the drag coefficient predicted by considering the group fixed (no-slip condition) is significantly higher than that predicted by a moving ground (slip condition). This may be one of the reasons for the difference in the observations between the present study and that of Hsuin *et al.*[1] It should be noted that the trends predicted by the present study (reduction in drag closer to the ground) agree with the observations made by Steinbach[2] from the experimental studies on ground effect.

5. Ground effect studies on multielement airfoil

The effect of ground on high-lift airfoils has been studied by considering a NACA 4412 airfoil with an external airfoil flap of NACA 4415. Both inviscid and viscous computations have been carried out for some typical range of parameters. Figure 3 shows the geometry details, a typical grid and some results for this case. From the present investigations, it can be concluded that for the two-element airfoil considered for moderate flop deflection angles the ground induces a positive effect on the lift characteristics of the high-lift airfoil chosen for the study and at higher angles of flap deflection. There is a decrease in the lift coefficient and increase in the drag coefficient near the ground.

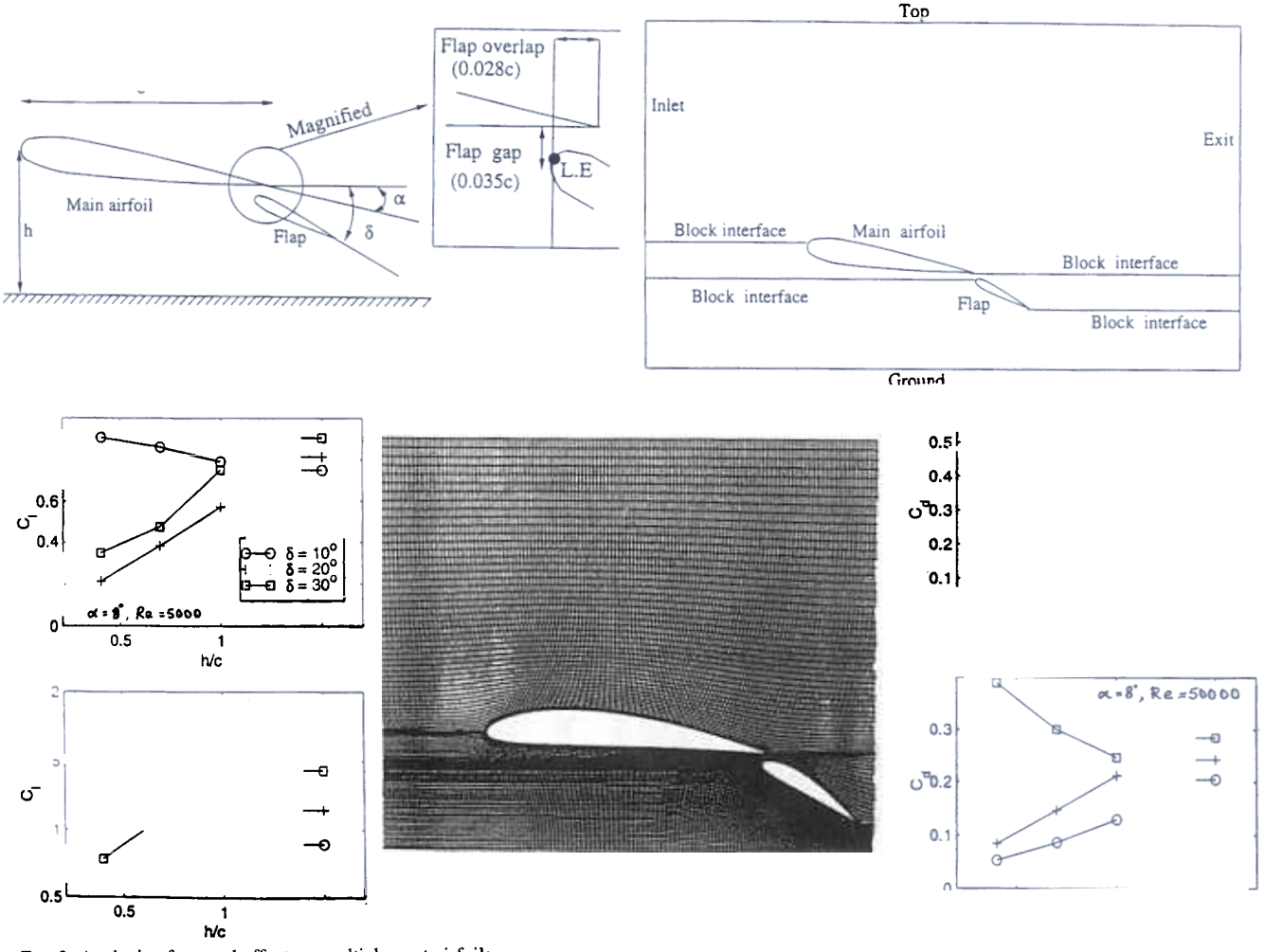

FIG. 3. Analysis of ground effect on multielement airfoils.

References

HSIUN, C. AND CHA' O-KUANG CHEN — Numerical investigation of the thickness and camber effects on aerodynamic characteristics for two dimensional airfoil with ground effect in viscous flow, *Trans. Jap. Soc. Aero. Space Sci.*, 1995, **38**, 77–90.

STEINBACH, D. — Comment on aerodynamic characteristics of a two-dimensional airfoil with ground effect, *J. Aircraft*, 1997, **37**, 455–456.

Thesis Abstract (Ph. D.

Modelling program dynamics: A study on locality of reference by K. V. Subramaniam
Research supervisor: Prof. T. Matthew Jacob
Department: Computer Science and Automation

1. Introduction

Locality of reference is a phenomenon exhibited by programs and computer systems in general, and refers to the tendency to localise operations to a small subset of the available resources. In the past, this phénomenon has been studied in terms of temporal and spatial locality;[1] studies of locality have been restricted to simple considerations that can be readily exploited to gain performance improvements. The objective of this work is to provide a general framework based on which locality studies can be conducted at various levels of detail work and investigate how this view can lead to improvements in design and evaluation methodology.

2. General principle of locality

Blevins and Ramamoorthy[2] proposed a General Principle of Locality (GPL) which we have further refined in order to arrive at a more general one. Our GPL asserts that in a system displaying locality of reference, (i) there will be nonuniform demand for resources, (ii) the demand patterns will be correlated over time, and (iii) if the demand pattern becomes uncorrelated over an interval, this signifies a transition in locality. Transitions demarcate *phases* of locality behaviour. We classify resources as *intrinsic* or *extrinsic*, depending on the level at which the study is performed, and show that spatial locality is merely an artefact of the mapping between intrinsic and extrinsic resources. Based on GPL and our classification of resources, we propose necessary conditions that must be satisfied by a model locality to be representative; we require that a representative model be able to accurately predict performance on various direct mapped cache configurations. Further, none of the published models of program memory behaviour, when evaluated based on our necessary conditions, was found to be representative.

3. Identifying locality phases

We started our modelling approach by identifying *locality phases* in the program. We used address traces of benchmarks from both the SPEC 92 suite (e.g. *cc1, compress, espresso, xlisp* and *mdljdp2*) and the Olden benchmark suite (e.g. *voronoi, tsp* and *bisort*). The traces were generated on an MIPS R4000 processor using the pixie utility.[3] Freiberger *et al.*[4] proposed an algorithm based on extrinsic resource usage which we found unsuitable for use in identifying phase behaviour. In contrast, the Bounded Locality Interval (BLI) method proposed by Madison and

Batson[5] uses intrinsic resources. However, in a data address stream, information about intrinsic resources, i.e. data structures, is not present.

3. *Dynamic data clusters*

We introduced the concept of dynamic data clusters, which are formed by partitioning a data reference stream. All data addresses in an address stream that are generated by the same base register producing instruction are associated with the same cluster. We found that using dynamic data clusters as intrinsic resources with the BLI method resulted in accurate identification of phases.

3.2. *Structural prefetch scheme*

A variation of this partitioning procedure forms the basis for the design of a hardware unit for prefetching structural references in a program. References in an address trace can be classified into strided, zero-strided and structural. Strided references result when an instruction accesses data addresses with a fixed stride. Zero-strided references are a special case of strided references when the stride is zero; this corresponds to scalar variable accesses. Structural references are generated as a result of traversal of some data structure and show no apparent pattern when analysed in isolation of the program code. We develop our prefetching scheme for structural references by associating a spatial footprint[6] with every base register producing instruction. Our evaluation of this structural prefetch scheme shows that it can reduce miss ratios by as much as 50%. Performance improves by as much as 75% when this scheme is used along with a strided prefetch scheme.[7]

4. Locality model

We developed a representative locality model for memory behaviour in a program phase, based on the GPL necessary conditions.[8] The parameters of our model are listed in Table I. The model was validated by comparing the cache miss ratios of a synthetically generated trace based on the model against miss ratios for the corresponding phase of the actual program, across various direct mapped cache configurations.

In embedded real-time systems, where the program is well known, it is possible to tailor the hardware design to meet the performance requirements of the application on this system. We demonstrated an application of the representative locality model by using it to design direct mapped caches to meet a target performance.

5. Fast LRU stack processing

The processing of the LRU stack,[9] used in our model, is known to suffer from performance problems. We presented four algorithms to speed up LRU stack processing and show that one of them, the Successive Depth Approximation algorithm, improves performance by as much as 50% over the best published algorithm which uses a splay tree to represent the stack.[10] The Successive Depth Approximation method uses a two-level data structure to represent the stack.

6. Conclusions

To summarise, this thesis makes the following contributions:

Table I
Description of model parameters

Parameter	Description
	Page size used for the model.
	Number of pages accessed in the phase.
	Number of references in the phase.
	Fraction of pages that are preferred pages, i.e. frequently accessed.
	Relative frequency of accessing a preferred page.
	Fraction of pages that are neglected pages, i.e. infrequently accessed.
	Relative frequency of accessing a neglected page.
	Relative frequency of accesses in a given *pageclass* where successive accesses to an offset are by the same page. *pageclass* is either preferred, normal or neglected. This is used to model nonuniformity of address reuse in the trace.
$P_{pagelru}(x)$	Distribution of LRU stack depths for pages. Modelled using a combination of hyperbolic distributions.
$P_{offdist}(x)$	Distribution of offset spatial distances. Offset spatial distance is computed as the absolute difference between two successive offsets accessed by the same page. Modelled using a combination of hyperbolic distributions.

- A broader perspective on the phenomenon of locality of reference, identifying the impact of resource mapping on manifestations of locality.
- A change in perspective of looking at locality by visualising locality in a broader sense.
- Classification of resource being the key to the effectiveness of a locality study.
- The concept of dynamic data clusters as a new partitioning approach for viewing address streams.
- A novel prefetch scheme for linked data structures, exploiting locality identified at the program structure level.
- An accurate and representative locality model of memory referencing behaviour.
- A performance target-based approach to design of cache memories.
- Fast algorithms to process the LRU stack.

References

HENNESSY, J. L. AND PATTERSON, D. A. *Computer architecture: A quantitative approach,* Morgan Kaufmann, 1990.

BLEVINS, P. R. AND RAMAMOORTHY, C. V. Aspects of a dynamically adaptive operating system, *IEEE Trans.*, 1976, **C-25**, 713–725.

3. SMITH, M. D. *Tracing with pixie,* Technical Report CSL-TR-91-497, Computer Systems Lab, Stanford University, Nov. 1991.

4. FREIBERGER, W. F., GRENANDER, U AND SAMPSON, P. D. Patterns in program references, *IBM J. Res. Dev.*, 1975, **19**, 230–243.

MADISON, A. W. AND BATSON, A. P. Characteristics of program localities, *Commun. ACM*, 1976, **19**, 285–294.

KUMAR, S. AND WILKERSON, C Exploiting spatial locality in data caches using spatial footprints, *Proc. 25th ACM/IEEE Int. Symp. on Computer Architecture*, 1998, pp. 357–368.

BAER, J. AND CHEN, T. F. An effective on-chip preloading scheme to reduce data access penalty, *Proc. 18th ACM/IEEE Int. Symp. on Computer Architecture*, 1991, pp. 176–186.

SUBRAMANIAM, K. V. AND THAZHUTHAVEETIL, M. J. Program memory access characteristics, *Proc. Fifth Int. Conf. on Advanced Computing*, Dec. 1997.

MATTSON, R. L., GESCEI, J., SLUTZ, D. R. AND TRAIGER, I. L. Evaluation techniques for storage hierarchies, *IBM System J:*, 1970, **9**, 78–117.

10. SUGUMAR, R. A. *Multi-configuration simulation algorithms for the evaluation of computer architecture design*, Ph. D. thesis, Department of Electrical Engineering and Computer Science, University of Michigan, Ann Arbor, 1993.

Thesis Abstract (Ph. D.

Asynchronous distributed rate control algorithms for best-effort sessions in integrated services networks with minimum rate guarantees by Santosh P. Abraham
Research supervisor: Prof. Anurag Kumar
Department: Electrical Communication Engineering

1. Introduction

Packet switching networks provide a best-effort transport service that is typically used by store-and-forward applications such as e-mail, file transfer and 'web' browsing. In an Integrated Services Packet Network, the best-effort sessions share the bandwidth that is left over after serving the guaranteed service traffic; further, this residual bandwidth needs to be shared fairly between the existing best-effort sessions. Since such sessions are controllable, a feedback control is used to modulate the emission of packets from the best-effort sources.

In this work, we are concerned with the problem of distributed rate control of best-effort sessions. Our motivation comes from the definition of the Available Bit Rate (ABR) service in Asynchronous Transfer Mode (ATM) networks. The problem we deal with has the following features:

An arbitrary network topology with a fixed configuration of best-effort sessions.

The sources transmit at a rate that is governed by explicit rate feedbacks from the network.

The link capacities (or bandwidths) available to the best-effort sessions are stochastically varying. There are rapid small variations, and in-frequent large variations in the link bandwidth, the former being caused by rate variations in guaranteed Variable Bit Rate sessions, and the latter by the arrival or departure of large guaranteed service sessions.

A form of max-min fairness is enforced between the sessions. Sessions can request a minimum rate (Minimum Cell Rate (MCR) in the ABR terminology).

The sources intersperse their data cells (packets) with Resource Management cells, which serve to carry control information between the network and the sources.

2. Contribution of the thesis

We begin by developing a notion of max-min fairness with minimum rate guarantees. This is a natural generalisation of the corresponding notion without such rate guarantees.[1] The basic theory for the original concept of max-min fairness is extended, and a centralised algorithm for obtaining max-min fair rates with minimum rate guarantees is obtained and proved. Another outcome of this development is a property of the max-min fair allocation that is useful for the development of distributed control algorithms. We show that the max-min fair allocation problem can be formulated as the solution of a certain nonlinear vector equation; the equation depends on the network topology, the session configuration and the link capacities. In this formulation, we associate a parameter with each link, called the link control parameter (LCP). A session obtains its rate by taking the minimum of the link control parameters along the links the session uses and comparing it with the session's minimum rate requirement. If the minimum of the link control parameters along the session's path is larger than the session's minimum rate requirement, then the session's rate is the minimum of the link control parameters along the session's path; otherwise, the session's rate is simply the minimum requirement. We prove that, given each session computes its rates as outlined above, the max-min fair allocation is obtained by the link control parameters that maximise utilisation of the links' capacities while keeping the flows through each link lesser than or equal to the link capacity. This requirement can be captured as the root of a nonlinear vector equation in the LCPs. Our approach to obtaining distributed algorithms consists of constructing algorithms that search for the root of this nonlinear vector equation. In such a distributed algorithm each link computes its link control parameter to maximise its total flow exceeding its capacity.

We begin our investigation into distributed algorithms by considering a model consisting of an arbitrary network topology with fixed session configuration and fixed link capacities. Generalising upon two existing algorithms, viz. Hayden's algorithm[2] and the UT algorithm,[3] which did not consider MCRs, we develop a generic distributed synchronous algorithm that incorporates MCRs. Like the Hayden's and UT algorithms, the generic distributed algorithm is implemented at each link. It updates the link control parameter from comparison of the link's capacity to the total flow through the link. The generic algorithm also captures the following useful features of Hayden's and UT algorithms.

The algorithm performs autonomous updates at the computing nodes with no explicit communication between the computing nodes.

The algorithm is not required to discriminate between the flows of individual sessions and hence does not need to maintain per session information.

We analytically prove that the rate allocations for the sources, computed by this generic algorithm converge to the max-min fair allocations. We then show that Hayden's algorithm which has an additive increment/decrement at each iteration and the UT algorithm which has a multiplicative increment/decrement at each iteration, enhanced to incorporate MCRs, are special cases of the generic distributed algorithm. The convergence proof allows for different links to imple-

ment different special cases of the generic update function, and still retains the convergence property.

A realizable distributed algorithm for the control of best-effort traffic must be robust to the following features of any communication network.

1. Asynchrony in the update epochs at different switching nodes due to different and possibly random update intervals.
2. Propagation delays which would cause delay response of a source to the control computed at a remote link.

The assumptions of a synchronous framework would be violated in such an environment. However, a distributed synchronous iterative algorithm that searches for the root of a vector equation can be adapted to operate in an asynchronous environment by one or both of the following methods.

Choose suitable large update intervals at the computing nodes to compensate for the delays.

Scale the increment/decrement at each iteration and/or use updates computed several update epochs before and not only the just previous iterate.

We present two algorithms that handle asynchrony and delays for the case where the link capacities are assumed to be fixed. The first algorithm uses a scaled increment/decrement at each iteration. The scaling factor is obtained using a heuristic. In the second algorithm, we use a moving average of the previous computed link parameters and a scaled increment/decrement. We analytically prove convergence of the second algorithm.

We then consider the case of stochastic available link capacities with rapid variations. The 'solution-of-equations' perspective enables us to formulate the distributed control problem as the solution of a vector equation given noisy observations. We propose a distributed stochastic approximation algorithm[4] for the solution of this problem. A stochastic approximation update consists of scaling the increment/decrement at each interation by a sequence of suitably chosen decreasing gains. Due to the decreasing gains, the effects of noise are suppressed. It has been shown[5] that the decreasing gains also suppress the effects of asynchrony and delays, thus retaining the convergence properties in an asynchronous distributed computing environment. We adapt the framework of Borkar[5] to our problem and prove that the session rates obtained converge to their max-min fair rates in spite of asynchrony and delays. The proof involves the standard procedure of showing that the evolution of the iterates emulate the solution of an ordinary differential equation (ODE). The steady-state solution of the ODE is shown to yield the max-min fair rates. The distributed stochastic approximation algorithm retains the desired structure of autonomous updates without explicit communication between the computing nodes.

Until this point in our work, the available link is viewed as a given quantity (in the stochastic case, the capacity is viewed as this given quantity plus noise). Thus the algorithms are purely rate-control algorithms, with no attention being paid to buffer occupancies at links, and probabilities of buffer overflow. We incorporate this aspect by appropriately defining the available

capacity of a link so that if the sources adapt themselves to this rate, then the buffer overflow probability would be small. Clearly, the mean of the capacity process a link would not do, since adapting the total flow of best effort traffic to the mean of the available capacity would cause large queue buildups at the nodes of the networks. We consider the problem of computing the constant input rate into a queue with a stochastic service rate that ensures that for a given threshold, the probability of the queue length exceeding this threshold is below a desired quantity. The formulation we use is the dual of the equivalent bandwidth formulation for sources with stochastic sending rates.[6] The equivalent bandwidth formulation involves the log-moment-generating function of the source sending rate. In the dual problem, we are concerned with the log-moment-generating function of the service rate. We propose two online estimation algorithms that estimate this input rate, which we call the equivalent service capacity (ESC) of the link. The first algorithm we propose consists of estimating the log-moment-generating function of the service process via empirical averages. An iterative procedure is outlined for computing the estimate. In the second approach we formulate the problem of finding the ESC as one of searching for the root of a certain function of the input rate that involves the given buffer threshold and probability of crossing this threshold at the input rate. The function requires an estimate of the probability of event of the queue length crossing the given threshold. Such as estimate cannot be accurately obtained using measurements over short intervals since the given threshold is large in general, and hence the event of crossing this threshold is a rare one. We propose an innovative technique in which accurate estimates of the function can be obtained by estimating the probabilities of crossing two smaller buffer thresholds. Since these two thresholds are smaller, accurate estimates of the desired probabilities can be obtained in short measurement intervals. In this technique, a stochastic approximation procedure is used to iteratively compute the ESC estimates. The performance of the proposed algorithms is demonstrated by simulation.

Finally, the distributed stochastic algorithm developed is put together with the available capacity estimation technique and simulations are run to study the whole approach. At this point, some heuristics are developed for adapting to large changes in the link capacities (such as those that could be caused by arrivals or departures of guaranteed service sessions). We find that the algorithm tracks the theoretically calculated max-min fair rates; further, the equivalent service capacity approach succeeds in limiting cell losses while avoiding the arbitrariness of simply using the mean link capacity times some factor such as 0.95.

References

BERTSEKAS, D. AND GALLAGER, R. G. *Data networks,* Prentice-Hall, 1987.

HAYDEN, H. P. *Voice flow control in integrated packet networks,* Master's thesis, MIT, Cambridge, Oct. 1981.

3. FULTON, C., SAN-QI LI AND LIM, C. S. UT: ABR feedback control with tracking, *Proc. IEEE INFOCOM'97,* Apr. 1994, pp. 806–815.

KUSHNER, H. J. AND YIN, G. G. *Stochastic approximation algorithms and applications,* Springer-Verlag, 1997.

BORKAR, V. Asynchronous stochastic approximation, *SIAM J. Control Optim.,* 1998, **36**, 840–851.

6. DE-VECIANA, G. AND WALRAND, J. Effective bandwidths: Call admission, traffic policing and filtering for ATM networks, *Questa,* 1995, **20**, 37 - 59.